Journal of Applied Fluid Mechanics, Vol. 16, No. 12, pp. 2381-2395, 2023.
Available online at www.jafmonline.net, ISSN 1735-3572, EISSN 1735-3645.
https://doi.org/10.47176/jafm.16.12.1996

Experimental and Numerical Investigation of the Control of the Flow Structure on Surface Modified Airfoils

A. Öztürk†, M. Çoban and F. Koca

Sivas Cumhuriyet University, Sivas, 58100, Turkey

†*Corresponding Author Email: aozturk@cumhuriyet.edu.tr*

ABSTRACT

In this study, experimental and numerical flow analysis was performed on three different blade profiles with a chord length of 165 mm using passive flow control method. The first of the airfoil is the standard NACA 0018 profile. The second airfoil type has a NACA 0018 profile with a gap in the suction surface. The last airfoil is the NACA 0018 profile which is 66% of the trailing edge cut from the chord length. All airfoil profiles were analyzed at the Reynolds number, $Re=2x10^4$, and angles of attack $\alpha=0^o$, 5^o, 10^o, 12^o and 14^o in both experiment and numerical studies. The experiments were carried out using the Particle Image Velocimetry (PIV) method in a closed-loop open water channel, and the time-averaged velocity vectors, streamlines, and vorticity contours of the flow field were obtained. Subsequently, numerical analyses were performed using the ANSYS Fluent package program, one of the Computational Fluid Dynamics (CFD) programs used frequently in the literature. The streamlines and pressure contours of the airfoil profiles have been compared visually at the same Re and different angles of attack. In addition, according to the angle of attack of the airfoil profiles, lift coefficient C_L, drag coefficient C_D, and the ratio of lift coefficient to drag coefficient C_L/C_D graphs were presented. It has been shown that the gap on the airfoil at high attack angles caused changes in lift (up to 0.7) and drag (up to 0.15). These features can allow these models to be used for different purposes in the aerodynamics field.

Article History

Received May 15, 2023
Revised August 10, 2023
Accepted August 13, 2023
Available online October 8, 2023

Keywords:

PIV
CFD
Airfoil
NACA 0018
Passive Flow Control

1. INTRODUCTION

An airfoil is defined as the cross-section of a body placed in an airstream to produce a useful aerodynamic force in the most efficient manner possible (Rubel, et al. 2017). Airfoil profiles made of different sizes and materials have a wide range of applications in both engineering and industry such as marine engineering, aircraft blades, fans, wind turbine blades, propellers, Unmanned Aerial Vehicles (UAV), Micro Aircraft Vehicles (MAV). Nowadays, especially when the aviation industry is developing rapidly, studies of flow on airfoil profiles have increased in order to increase airfoil efficiency (evaluated with the lift to drag ratio (L/D)). Flow on an airfoil is important for determining drag and lift characteristics, particularly at angles of attack and different speeds. The performance of the airfoil profile can be easily increased by changing the profile structure according to the application. One of the objectives of the studies on flow control methods is to delay flow separation. If the point at which the flow leaves the surface is closer to the trailing edge, the flow will be more regular. This means that the lifting of the wing increases, and the resistance decreases. The methods used in the studies to delay this separation and bring it closer to the trailing edge are divided into active and passive flow control methods. While a mechanism is used in the active flow control method to control the flow characteristics, the passive flow control method is applied by using the own geometry of the airfoil. This method applied with changes in geometry is known as the passive flow control method, and there is no need for a mechanism used to control flow as in active flow control. In recent years, studies on flow control methods have increased (Belamadi et al., 2016; Hoogedoorn et al., 2010; Luo et al., 2017; Yang et al., 2017). In addition, active and passive control methods are not only in airfoils but also in many different studies (Joshi & Bhattacharya, 2019, Bhattacharya & Gregory, 2015; Koca & Ozturk 2022). The changes in geometry should be calculated from the angle of attack, leading-edge, trailing edge, span length, chord length, lift force, drag force, and thickness all from the geometry of the wing clearly defined. Various studies have been carried out to improve

NOMENCLATURE			
c	airfoil chord length	Re	Reynolds number
C_D	drag coefficient	V	free stream velocity
C_L	lift coefficient	$<V>$	velocity vectors
F_D	drag force	$<\omega>$	vorticities
F_L	lift force	$<\Psi>$	streamlines
CFD	Computational Fluid Dynamics	α	angle of attack
PIV	Particle Image Velocimetry		

the performance of airfoils, and in these kinds of studies, numerical modeling or experimental methods have been used frequently (Esfahani et al., 2015; Wang et al., 2017; Zhang et al., 2017; Jawahar et al., 2018, Guoqiang et al., 2019; Anzalotta et al., 2020; Sun et al., 2021). Luo et al. (2017) studied the effect of passive flow control numerically using a micro cylinder near the leading edge of a stalled airfoil (NACA 0012) between 16º and 23º angles of attack at a $\mathrm{Re} = 6\mathrm{x}10^6$. According to obtained results, they have not proposed to control locations near the pressure surface of the airfoil among the 15 locations of the microcylinder investigated in their study. In the studies of Sreejith and Sathyabhama (2018), the flow behavior of laminar flow separation on an E216 airfoil at different angles of attack was numerically investigated at $\mathrm{Re} = 10^5$. Numerical results have been verified by experimental results obtained in the wind tunnel. It was observed that the maximum improvement in the drag coefficient was 15.48%, and the lift coefficient was 21.62% at the angle of attack of α = 6º. He et al. (2016) conducted aerodynamic performance research having two-dimensional flow at $\mathrm{Re} = 7.76\mathrm{x}10^5$ by adding a gurney flap to the trailing edge of an SFYT15 thick type airfoil profile belonging to an aircraft operating in a free airflow environment of 25 m/s at 20 km altitude and having a chord length of 5 m. Especially in the gurney flap model with an angle of attack of 3º and a height of 0.5% of the wing chord, it was observed that the lift-drag ratio increased by 2.7%, and the lift coefficient increased by 12.9%. Fouatih et al. (2016) experimentally studied the flow separation control of a NACA 4415-type airfoil fitted with a vortex generator. Wind tunnel tests were performed and compared at different angles of attack and Re numbers. As a result of the study, it has been observed that the most effective generator in the control of boundary layer separation is the triangular-shaped generator placed in the middle of the chord with an angle of α = 12º and a distance of 3 mm between the generators. Belamadi et al. (2016) analyzed the effect of a slit on airfoil aerodynamics numerically by opening a slit in the middle of the airfoil in order to make boundary layer control in a Baseline S809 type airfoil profile. The slotted airfoil performed better than the normal profile at angles of attack between α = 10º and α = 20º in their study. Chounhry et al. (2015) conducted a study to better understand the effect and characteristics of a long flow separation protrusion on the flow around the airfoil, placed on the NACA 0021 airfoil at low Re number and turbulence density. The protrusion has been shown to increase the flow separation as the angle of attack increases. It has been observed that the increase in Re number or the level of turbulence reduces the negative effects of the protrusion and improves airfoil performance, and promotes the trailing edge stall effect. Genç et al. (2008) analyzed the forces on the airfoil numerically by applying a symmetrical flap to the NACA 0012. As a result, they have observed that flaps positively affect airfoil performance up to α = 15º angle of attack and decrease the L / D ratio by increasing the drag coefficient after 15º. Olsman et al. (2011) experimentally investigated the dynamic response of a NACA0018 airfoil with a cavity to the flow and acoustic forcing around it. They considered the NACA0018 profile with 2 different cavities and the airfoil without cavity. As a result of the study, they stated that the use of cavities especially in thick airfoil structures can be used to prevent acoustic resonance. Yadav and Bodavula (2021) numerically presented the effect of triangular space at low Reynolds number on the unsteady aerodynamics of NACA 0012. Right-angled triangular cavities are placed at 10%, 25% and 50% chord location on the suction and have depths of 0.025c and 0.05c, measured normal to the surface of the airfoil. They stated that while there was no flow instability between the gapped and gapless blades at small angles of attack, flow instability occurred at high angles of attack. However, they emphasized that deeper cavities reduce flow instability. Tanürün et al. (2020) investigated the NACA-0018 wind turbine blade model performance at different aperture ratios numerically and experimentally. As a result of the study, they stated the altitude loss angles of AR1 and AR2 wing models as 32.5° and 25°, respectively, and they reported it as 35° and 30°, respectively, in the results they obtained from the experimental study. Yavuz (2021) presented the flow and mechanical properties of a modified Naca blade geometry numerically. It was stated in the study that depending on the angle of attack, the pressure and flow effects on the wing cause higher bending-torsion effects and increase the stresses in the stabilisation region of the wing. In addition, it was reported that the lowest deformation and average stresses occur at the angle of attack of -4°.

Flow separation control, by means of passive devices, is today the less expensive and the quickest solution to implement. They can be used to control from low-speed separated flows in adverse pressure gradient to transonic shock-induced separation (Lin, 2002). In the case clearly stated in the literature, the structures of the airfoil profiles change the pressure area, resistance and accordingly the efficiency of the systems, the fuel and even the effects on the environment due to the fuel. Therefore, the design of the profiles of the airfoils is very important. In the present study, experimental and numerical flow analysis has been performed on three different airfoils with 165 mm chord length using the passive flow control method. The first of the airfoil is the standard NACA 0018 profile. The second type of airfoil has a NACA 0018 profile with a cavity in

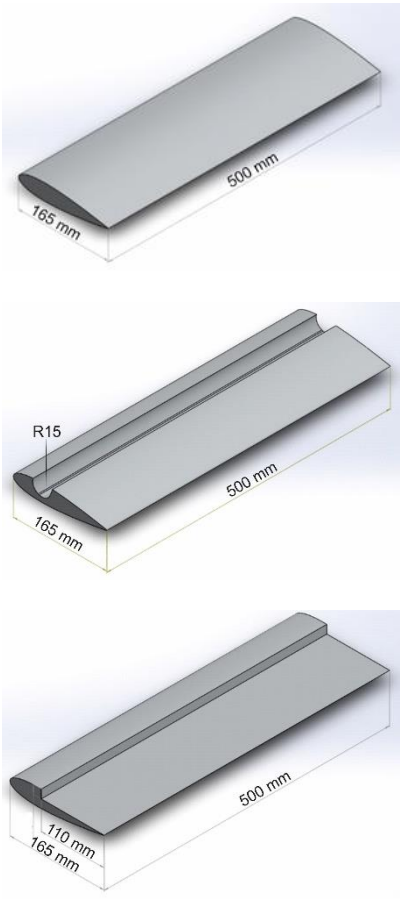

Fig. 1 General view of models used in this study a) standard NACA 0018 airfoil model b) gapped NACA 0018 airfoil model c) stepped NACA 0018 airfoil model

its suction surface. The last airfoil is the NACA 0018 profile which 66% of the trailing edge is cut from the chord length. The airfoils used in the study were chosen in this way in terms of their usability at high altitudes, both in terms of structural durability and ease of production. As a result, flow contours of the airfoil profiles have been compared visually at the same Re number and different angles of attack. In addition, according to the angle of attack of the airfoil profiles, lift coefficient C_L, drag coefficient C_D, and the ratio of lift coefficient to drag coefficient C_L/C_D graphs are presented in this study. Although there are many studies on airfoils, there is no study both experimentally and numerically standard stepped and gapped models are compared under the same conditions. With this study, it will be contributed to the literature and will be presented to the attention of researchers.

2. METHOD

In this study, three different wing models with 165 mm chord length were used. These models are as follows and shown in Fig. 1;

a) Standard NACA 0018 airfoil model with a symmetrical structure (*Standard Model*),

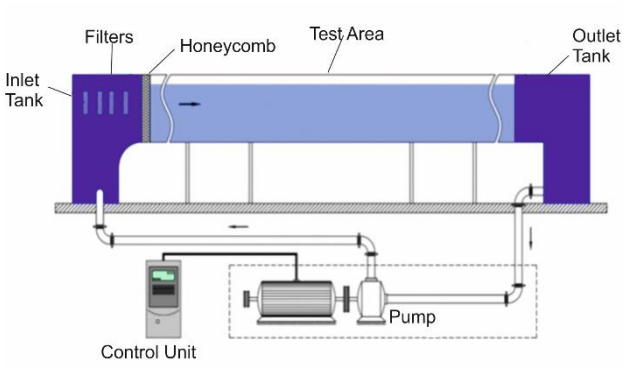

Fig. 2 PIV test water channel and equipment

b) Standard NACA 0018 airfoil model with circular gap (cavity, hollow) geometry, (*Gapped Model*). The center of the circle is at a distance of 70% (about 50 mm) from the trailing edge. In order that the flow can easily exit the cavity, it is inclined at an angle of 20º in the direction of the trailing edge from the radius (R = 15 mm) (Ozturk & Coban, 2014).

c) Standard NACA 0018 airfoil model in which cut is 66% (110 mm) from the trailing edge (*Stepped Model*). The step depth is taken up to the symmetrical cord.

2.1 Experimental Setup and Measurement Technique

PIV experiments were carried out in the closed-circuit open surface water channel established in the Fluid Mechanics Laboratory of Çukurova University, Mechanical Engineering Department, which is shown in Fig. 2. The water channel consists of two water tanks and a transparent measurement area of 750 mm x 1000 mm x 8000 mm (height x width x length) made of acrylic material between these two tanks. The flow rate in the channel is adjusted by a pump that can operate at different speeds with the help of a speed control unit. Models were placed in the channel by connecting from both ends to two 500 mm x 500mm apparatuses made of acrylic plate. Also, the angles of the attack were adjusted with the help of these plates. The Reynolds number based on the free channel velocity and the chord lengths was $2x10^4$. Both experimental restrictive situations and literature were taken into consideration in the determination of the Re number. As it is known, experimental studies have many restrictive situations. The most important of these restrictive situations is cost. In the PIV test mechanism used, the high Re numbers cannot be reached. Also in the literature, there are four Re regimes, i.e., the ultra-low ($<1.0\times10^4$), low (1.0×10^4–3.0×10^5), moderate (3.0×10^5–5.0×10^6), and high Re ($>5.0\times10^6$), are proposed based on their characteristics of the C_L-Re relationship and the flow structure (Counsil & Boulama, 2013). The Re is commonly less than 2×10^5 for MAVs, less than 1.5×10^4 for NAVs, and even lower for insect flights. So this study has been examined for Re $=2.0\times10^4$, which represents the low-Re regimes. The experiments were performed at for $Re=2x10^4$ with turbulence intensity ($I=u'/U$) of 0.5%. When comparing the numerical results with the experimental result, it is important to make the comparison at the same Reynolds number for the accuracy of the comparison. Therefore, the same turbulence

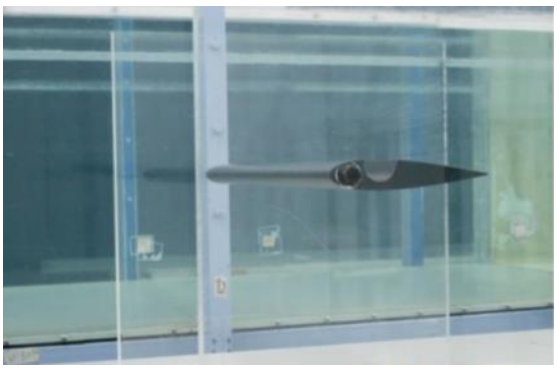

(a)

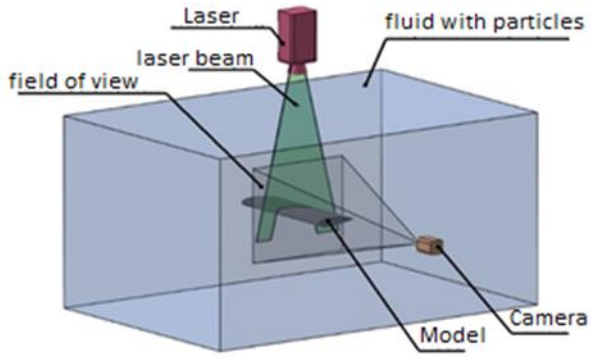

(b)

Fig. 3 a) Experimental, b) Schematic view of the water channel, camera, laser source and airfoil model

intensity of the experiment was considered in the numerical study.

In the PIV Experiments, the DANTEC PIV system, which consists of a 120 mJ Nd: YAG laser, a synchronizer, and a double pulsed laser system with a wavelength of 522 nm, was used. A digital camera with a maximum frame rate of 30 Hz and a spatial resolution of 1024 × 1024 pixels was also used for image recording with this laser system. Metallic-coated tracer particles of hollow plastic spheres with the same density as water, 14 µm in diameter, were mixed into the water flow and the movements of these particles were recorded. The gapped model in the water channel and the schematic of the experimental setup are given in Fig. 3. In the PIV experiments in this study, measurements were done in an area of 1200 x 1600 pixels. There is an angle with $\alpha = 90^{o}$ between the camera view and the laser beam. The laser beam was delivered from the upper part of the channel, and the camera was on the side. The beam coming from the laser unit was sent to the airfoil through a mirror placed on the channel at an angle of 45 degrees.

Models were made of aluminum material. Since the laser beam cannot pass through aluminum, the laser beam cannot illuminate the pressure part of the model. For this reason, the region at the bottom of the model is seen as dark. Since the effect of the airfoil modification surfaces on the flow structure is examined, there is no experimental drawback in staying dark in this pressure region. The models used in the experiment were designed for flow analysis in two dimensions (2D), and it was assumed that there were no changes in the third dimension due to the nature of the experiment designed, and that small changes would not affect the flow. Therefore, the laser beam was sent from the top of the channel to the middle part of the 500 mm long model. The blockage ratio should be chosen as small as possible to avoid extra load on the blade. On the other hand, in order to obtain a good image, it is desired to be of ideal size. The blockage rate for the largest angle of attack in the study is 1.4%.

2.2 Computational Setup

Many package programs have been developed to solve fluid mechanics problems. The ANSYS Fluent program, which is one of the frequently used programs and performs analysis based on finite volumes, was used for numerical analysis in this study. In computational fluid dynamics, the conservation equations in flow dynamics are used for the transition from one form to another. Mathematical models in the analysis are based on numerical solutions of mass, momentum and energy equations.

The conservation of mass equation is as follows:

$$\frac{\partial \rho}{\partial t} + \nabla.\left(\rho \vec{v}\right) = S_m \tag{1}$$

Equation (1) is the basic form of the conservation of mass equation and is valid for both compressible and incompressible flows. If the mass is not added from the dispersed second phase (e.g., due to evaporation of the liquid droplet), the source S_m equals zero.

The momentum equation is as follows:

$$\frac{\partial}{\partial t}\left(\rho \vec{v}\right) + \nabla.\left(\rho \vec{v}\vec{v}\right) = -\nabla p + \nabla.\left(\bar{\bar{\tau}}\right) + \rho \vec{g} + \vec{F} \tag{2}$$

where p is the static pressure, $\bar{\bar{\tau}}$ is the stress tensor, and $\rho\vec{g}$ and $\vec{F}$ are the gravitational body force and external body forces, respectively. Here, the physical magnitude of gravity is much smaller than other forces, such as pressure and viscous forces. So, it was not considered in the study since it has no significant impact on the results. An external force is a force acting on the system from the environment due to external agents. In other words, an external force is a force that acts from the outside. An external force that does work on a system changes the momentum of the system. These can cause a change in position, velocity, or acceleration of the system. An isolated system is one for which the sum of the average external forces acting on the system is zero. The study is also considered an isolated system.

Surface modifications are created on an airfoil (such as hollow and stepped patterns), as well as changing angles of attack resulting in higher turbulence. In addition, the turbulence intensity was measured as 0.5 during experiments. Therefore, it was decided to use the most suitable turbulence model in the numerical predictions to reveal turbulence effects.

The standard $k-\omega$ turbulence model, one of the frequently preferred models in similar studies in the literature, was used for all numerical analyses in this study. The standard $k-\omega$ model is an empirical model

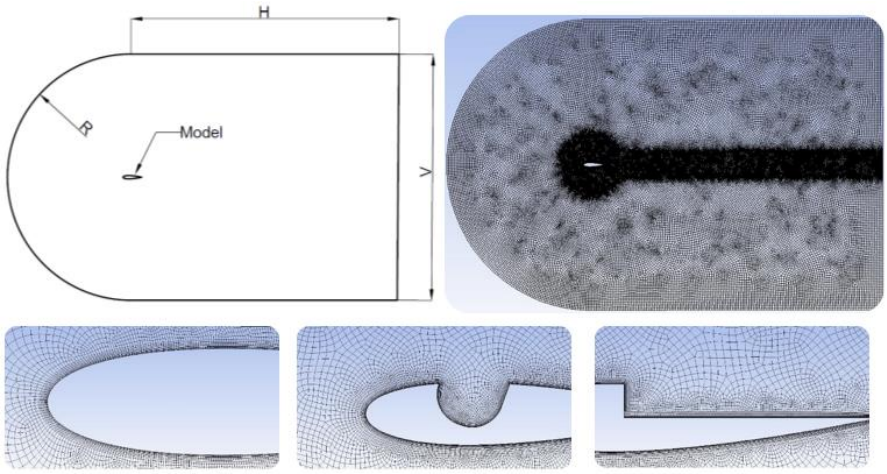

Fig. 4 C-H and mesh structure views

based on model transport equations for turbulent kinetic energy (k) and a specific diffusion rate (ω). From the RANS modeling point of view, the k − ω model offers several advantages relative to the k − ε model. The most important one is that the equations can be integrated without additional terms through the viscous sublayer. Furthermore, the k − ω model is typically better at predicting adverse pressure gradients for boundary layer flows and separation (Han & Krajnović, 2015). Kinematic eddy viscosity, turbulence kinetic energy, and specific dissipation rate are as follows (Wilcox, 1988):

$$v_T = \frac{k}{\omega} \tag{3}$$

$$\frac{\partial k}{\partial t} + U_j \frac{\partial k}{\partial x_j} = \tau_{ij} \frac{\partial U_i}{\partial x_j} - \beta * k\omega + \frac{\partial}{\partial x_j}\left[\left(v + \sigma * v_T\right) \frac{\partial k}{\partial x_j} \right] \tag{4}$$

$$\frac{\partial \omega}{\partial t} + U_j \frac{\partial \omega}{\partial x_j} = \alpha \frac{\omega}{k} \tau_{ij} \frac{\partial U_i}{\partial x_j} - \beta \omega^2 + \frac{\partial}{\partial x_j}\left[\left(v + \sigma v_T\right) \frac{\partial \omega}{\partial x_j} \right] \tag{5}$$

Closure coefficient and auxiliary relations used in Eq.3, Eq. 4 and Eq. 5: $= \frac{5}{9}$, $\beta = \frac{3}{40}$, $\beta^* = \frac{9}{100}$, $\sigma = \frac{1}{2}$, $\sigma^* = \frac{1}{2}$, $\varepsilon = \beta^* \omega k$

It is difficult to do algebraic processing each time to find out how an airfoil behaves at what angle of attack and Re numbers in terms of drag and lift. For this reason, there are non-dimensional expressions about the forces acting on the airfoil profiles. Dimensionless expressions for the Re number, the lift coefficient C_L, and the drag coefficient C_D are as follows:

$$\mathrm{Re} = \frac{\rho V c}{\mu} \tag{6}$$

$$C_L = \frac{F_L}{\frac{1}{2}\rho V^2 c} \tag{7}$$

$$C_D = \frac{F_D}{\frac{1}{2}\rho V^2 c} \tag{8}$$

Table 1 Dimensions of the C-H structure

Position	Length (mm)
Airfoil Chord	165
R	1090
H	2365
V	2180

Here, F_D represents the drag force, F_L represents the lift force, ρ is the fluid density, V is the fluid velocity, μ is the fluid viscosity, and c is the chord length in the above equations.

Numerical studies (assuming that the profile does not change with the airfoil span length) were made in 2D. The coordinates of NACA 0018 were taken from the database created by the "University of Illinois Applied Aerodynamic Group (UIUC Applied Aerodynamic Group)" and published at url-2 [32], then the coordinates were scaled to 165 mm. The new scaled coordinates were created using a Computer-Aided Design (CAD) program and then saved. The modified models were recorded in the same way. These profile surfaces were added to the Fluent in the ANSYS package program. The C-H type field was used because it is sufficiently far from the boundary layer and is frequently used in the literature. The C-H structure and the location point of the models used are shown in Fig. 4, and the dimensions of the C-H structure are presented in Table 1. Models are placed in the center of the C-shaped semicircle.

The rectangular form is used as a mesh structure close to the airfoil profile surface, and cells are formed in non-structural mesh geometries after a certain distance from the surface. The general mesh structure and the region where the mesh structure starts to get denser can be seen closely in Fig. 4. In order to better understand the appearance vorticity and different flow patterns, a fine mesh structure has been formed, especially at a certain distance from the surface. Similarly, after the trailing edge of the airfoil, the mesh structure has been formed relatively denser to better analyze the wake region and the part of the flow after the airfoil profile. For the use of an acceptable mesh structure, the results obtained from the

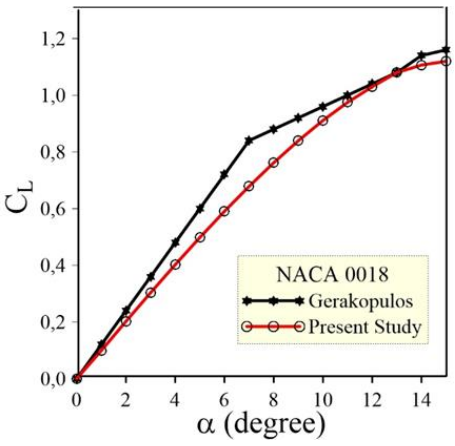

(a)

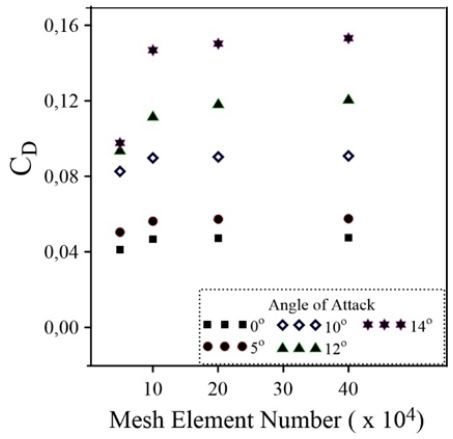

(b)

Fig. 5 a) Comparison of C_L results obtained in the present study and C_L, results of Gerakopulos et al. (2010) for different attack angles, b) C_D results for different angles of attack with different mesh element numbers

numerical analysis have been compared to the experimental study of the aerodynamic characteristics of the standard NACA 0018 model at low Re numbers and under the same conditions by Gerakopulos et al. (2010). The C_L results of Gerakopulos and this present study obtained with the 124.000 cell mesh structure are compared at different angles of attack, and the accuracy of the model is shown in Fig. 5 (a).

A grid independence study was performed as presented in Fig. 5 (b) to determine the minimum number of mesh elements required for the simulations. For this, the indicator output parameter C_D coefficient is taken. In the rule adopted as the rule of 1.2.4, the mesh element number is considered twice the value of the previous value and the result is reached. For example, the 1st mesh number is 100k, the second is 200k, the third is 400k, the 4th is 800k, etc. In this way, the number of meshes to be applied is obtained in a shorter time. Under the 1, 2, 4 rule, the mesh element numbers of $5x10^4$, 10^5, $2x10^5$ and $4x10^5$ were evaluated. Changes in C_D value in mesh element numbers of 10^5 and above were obtained as very low and acceptable. Based on this result, the analyses were made in $1{,}24x10^5$ mesh element numbers, taking into account the computer capacity and processing time.

The mesh for the airfoil geometry is of hybrid type. The cells of the meshes are quadrilateral and mesh matrix had orthogonal quality. The element is 50% of the chord and element order is linear. The edge sizing of the airfoil is bias type of bidirectional having bias factor of 10 and element size of 0.3% of chord. Smooth transition with 1.2 growth rate inflation has been taken near the surfaces of the airfoils. The layers of inflation are 10 and maximum thickness is 0.6% of the chord. For body sizing, a sphere of influence of radius of 300% of chord and element size of 5% of chord is taken where the center of radius of sphere of influence is at the origin of the global coordinate system.

The center of the first cell over the airfoil surface is located at a non-dimensional height of $y+\approx 1$.

The accuracy of numerical studies depends on both the mesh independence and validations. Considering this situation, mesh independence was achieved and validation analysis was started. The validation of numerical analysis is obtained by experimental studies. The comparison of both the experimental results and the comparison of the numerical results with the literature was conducted by the study of Gerakopulos et al. (2010). In this way, it was thought that the possible mistakes that may arise by using $2x10^4$ instead of taking Reynolds 10^5 would also be revealed. As a result of the validation, both the accuracy of the numerical study was revealed and it was a reference for experimental work. A velocity-inlet condition ($u=u_{inlet}$, $v=0$) was set at the domain inlet (semi-circular boundary) with a value that corresponds to a Re number of 20000 based on chord. At the domain outlet, a pressure-outlet condition equal to atmospheric pressure was set ($p=p_{atm}$). The airfoil was defined with the wall-boundary condition (no-slip, $u=0$, $v=0$), and the spanwise limits of the domain were set as a symmetry boundary condition.

In numerical analysis, the created models were made by changing the angle of attack. Air with a density of $\rho = 1.225$ kg / m^3 and a viscosity of $\mu = 1.7894 \times 10^{-5}$ kg / m.s was used as the fluid. Instead of angling the airfoil at every degree, the air directed on the airfoil as frequently used in the literature was sent at an angle. As in the experimental part, analyses were made for $Re = 2x10^4$ according to the chord length. The standard $k-\omega$ turbulence model is preferred in the analysis according to the literature (Orabi et al., 2020). Considering the PIV experiments, the turbulence intensity was chosen similarly (0.5%). For this reason, the fluid velocity profile coming to the wing surface is smooth. Equations were solved with the "Simple" algorithm, "green gauss node-based", and "second-order upwind" solutions were selected. The fluid was considered incompressible in the analysed Re number so that the energy equation was not taken into account since it would not affect the analysis results.

3. RESULTS AND DISCUSSION

In the experimental part of this study, the time-averaged velocity vector, $\langle V \rangle$, streamline, $\langle \Psi \rangle$ and vorticity contour, $\langle \omega \rangle$ distributions were obtained by using the PIV method in the vertical mid plane of the model airfoils.

The results of the experimental and numerical analyses were obtained at $Re = 2x10^4$ and angles of

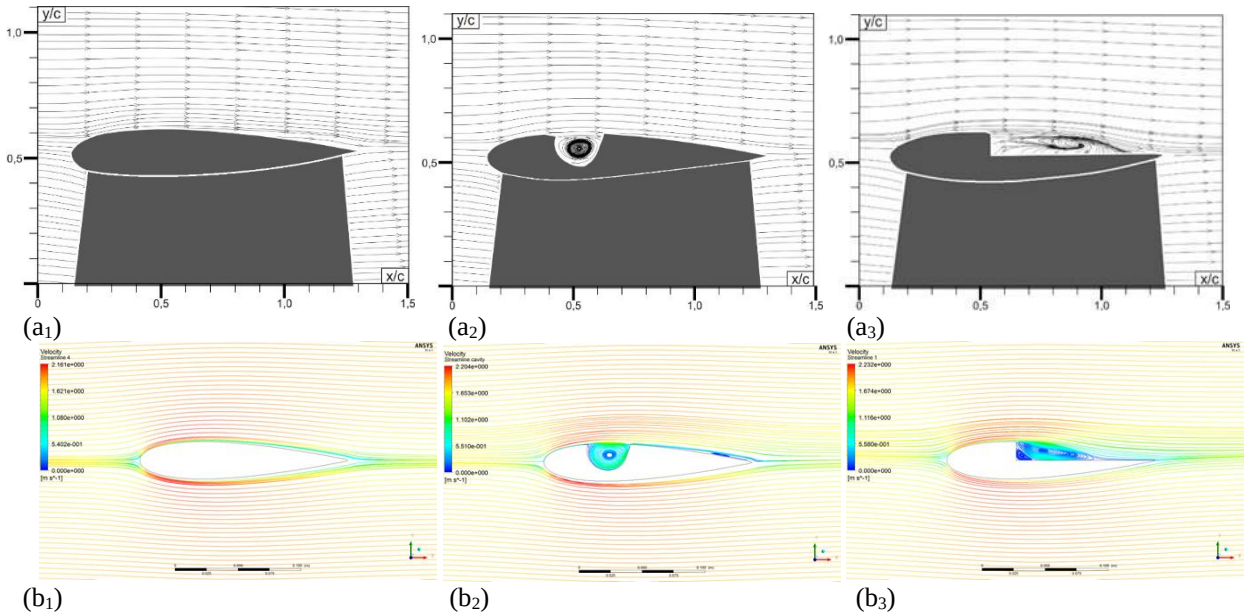

Fig. 6 Time-averaged patterns of streamlines at an angle of attack α = 0º (a) experimental, (b) numerical

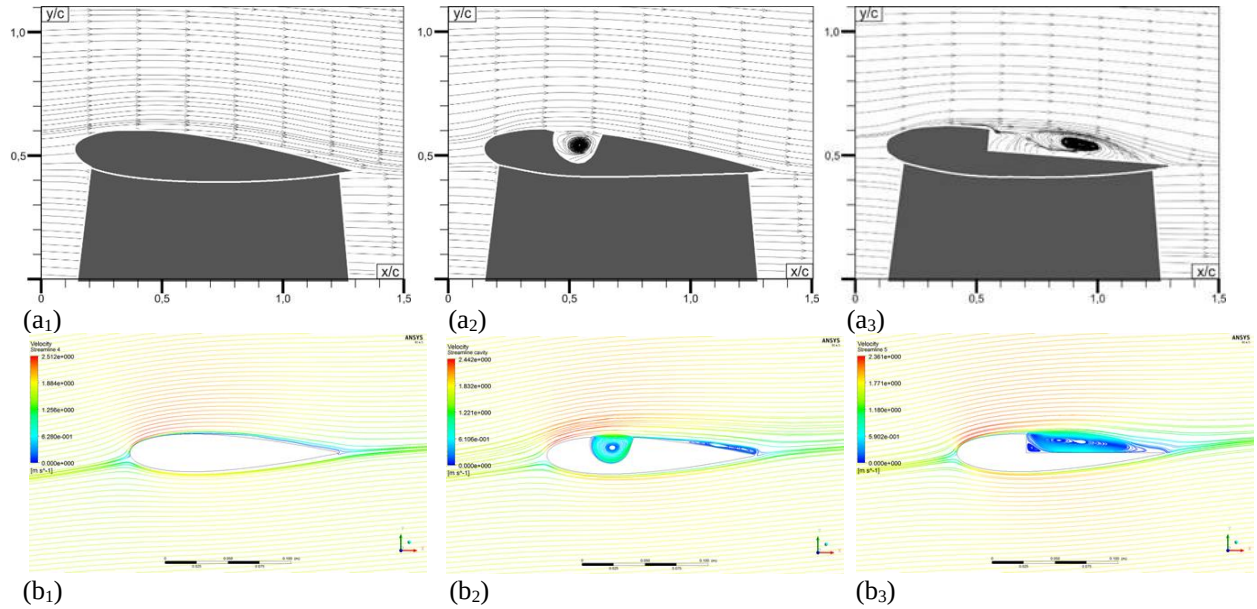

Fig. 7 Time-averaged patterns of streamlines at angle of attack α = 5º (a) experimental, (b) numerical

attack α = 0º, 5º, 10º, 12º and 14º. In Figs 6-10, the pattern of streamlines obtained from experimental and numerical analysis are given comparatively. Lower indis (1, 2, 3) represents standard, gapped, stepped models respectively. In the numerical study, the fluid flow angle was changed instead of turning the wing to change the angle of attack not to distort the mesh structure while obtaining streamlines and pressure contours. While experimental results are given on a dimensionless scale as y/c (distance /chord length) and x/c (distance /chord length), numerical results are given with the velocity gradient. When the pattern of streamlines is examined, as expected, the standard model does not have flow separation at small angles of attack. This situation continues up to the angle of attack of 12º experimentally and 10º numerically. This difference between them is thought to be due to the numerical analysis acceptance and the experimental uncertainty errors. The gapped model has a recirculation region at all angles of attack inside the cavity. A secondary circulation region occurred towards the airfoil trail edge with the increase of the attack angle. For the stepped model, there is a flow separation at all angles of the attack starting from the step line. While these separations tend to re-attach towards the airfoil trail edge at small attack angles, the increase in the angle of attack causes the vorticity to grow and their centres to replace towards the airfoil trail edge. It is clearly seen that the numerical results are consistent with the experimental results. Small differences arise from uncertainty errors that cannot be revealed in experiments and assumptions made in numerical studies (fixed fluid temperature, frictionless channels, etc.). Already in the literature, no numerical work cannot be demonstrated as the equivalent of experimental study. It is only emphasized that differences are acceptable by minimising.

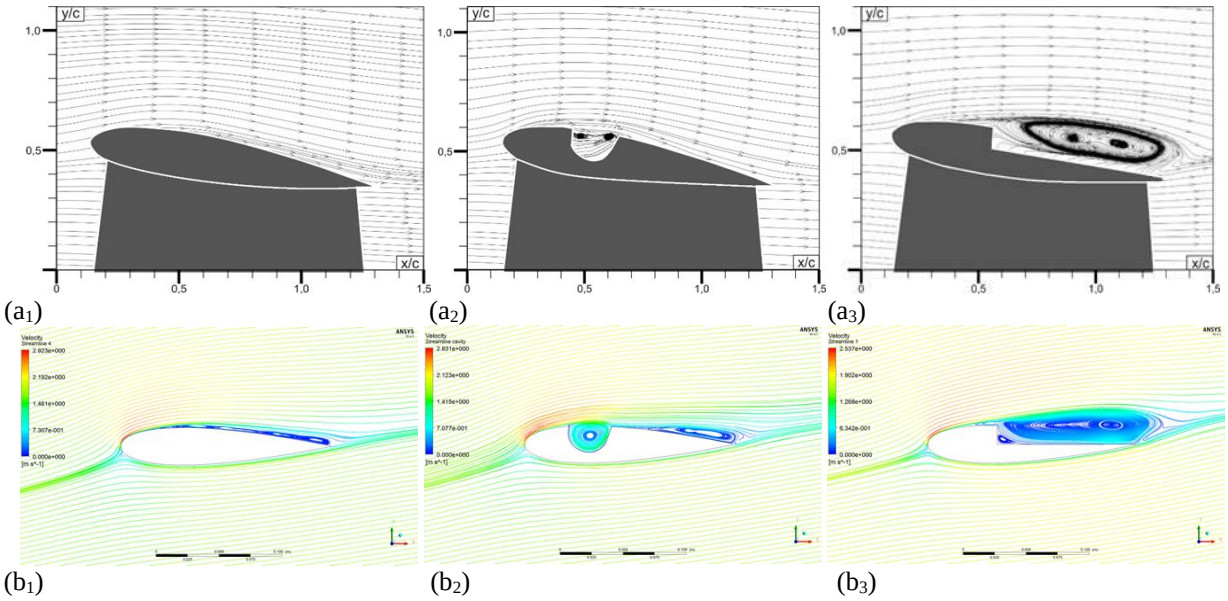

(a_1) (a_2) (a_3)

(b_1) (b_2) (b_3)

Fig. 8 Time-averaged patterns of streamlines at an angle of attack α = 10º (a) experimental, (b) numerical

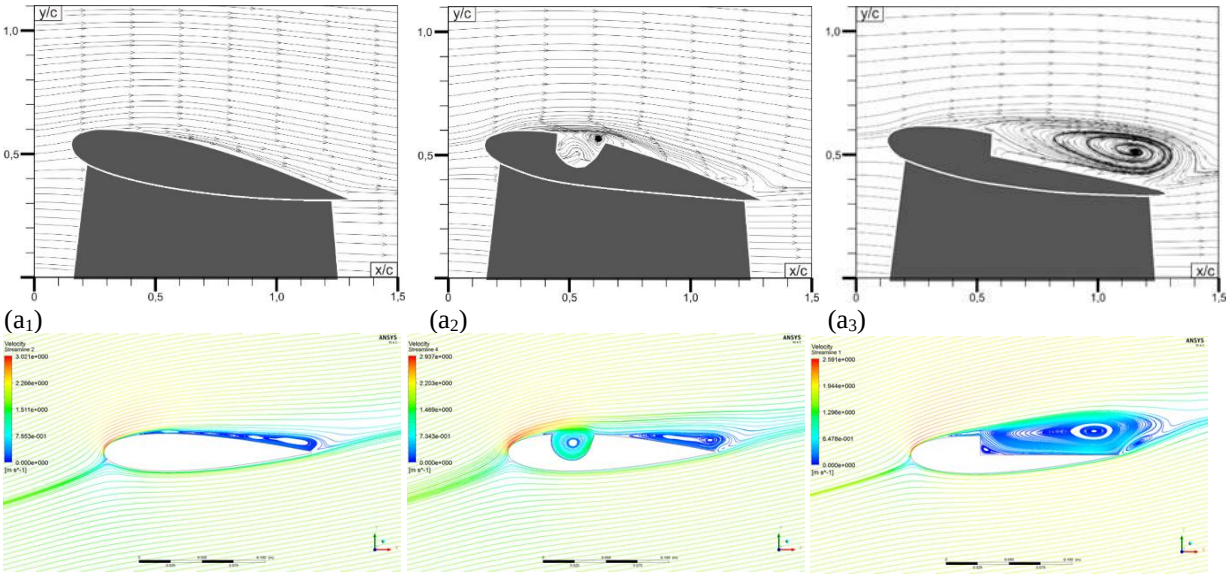

(a_1) (a_2) (a_3)

(b_1) (b_2) (b_3)

Fig. 9 Time-averaged patterns of streamlines at an angle of attack α = 12º (a) experimental, (b) numerical

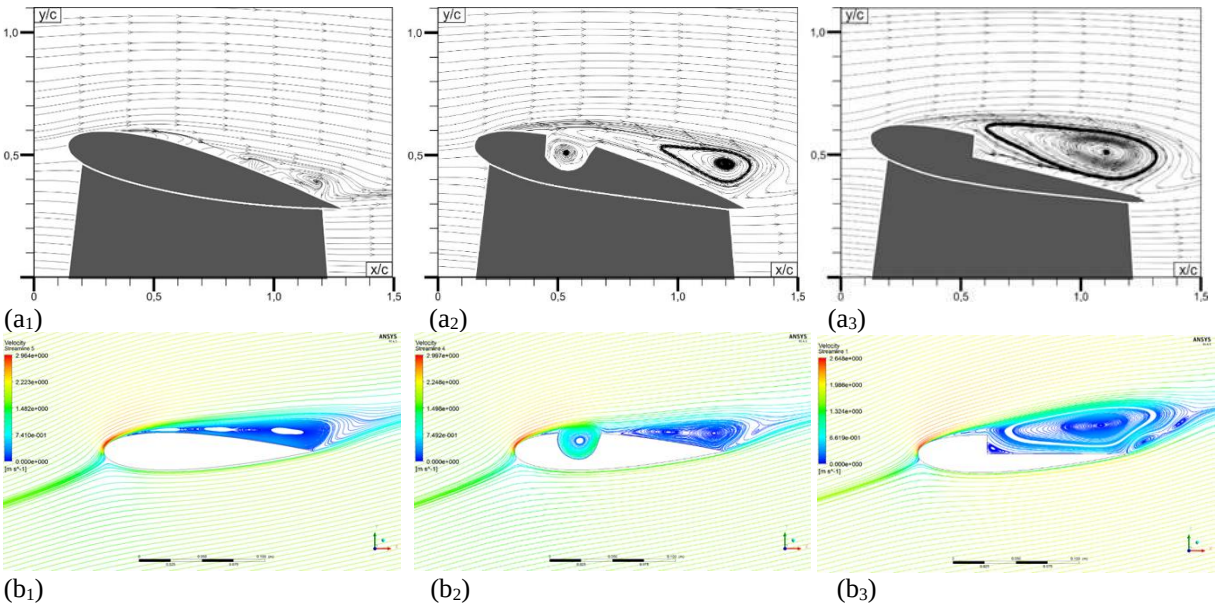

(a_1) (a_2) (a_3)

(b_1) (b_2) (b_3)

Fig. 10 Time-averaged patterns of streamlines at an angle of attack α = 14º (a) experimental, (b) numerical

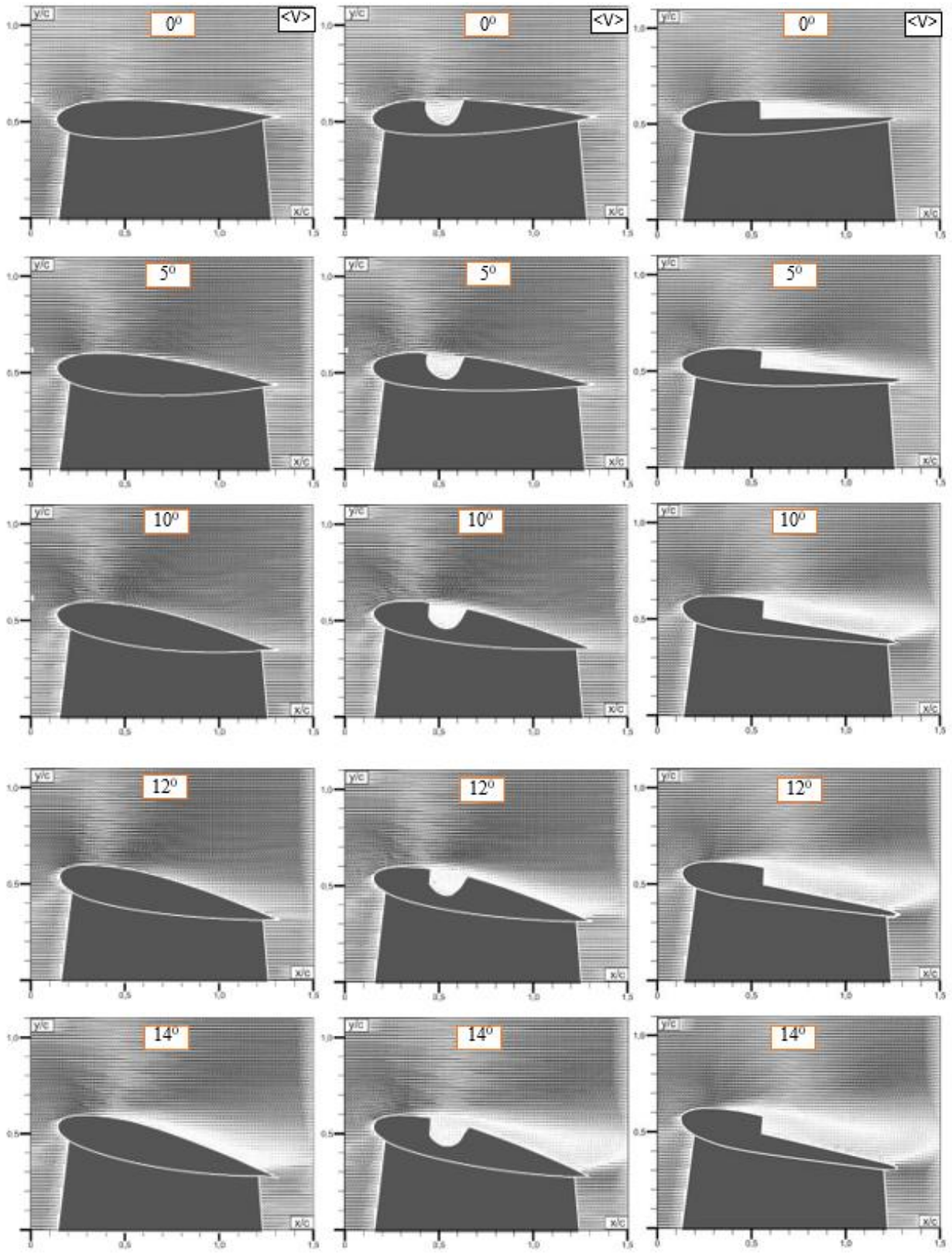

A B C

Fig. 11 Time-averaged velocity vectors at different angle attack of A) standard model, B) gapped model, C) stepped model

Velocity vector fields obtained from PIV measurements are given in Fig. 11. x and y axes are dimensionless according to airfoil chord length (c). According to the standard model, the velocity decrease in the modified parts of gapped and stepped geometries is seen as vectorial (velocity vectors). Besides, this situation is more pronounced with increasing angle of attack; it spreads over a wider area.

The time-averaged vorticity contours obtained experimentally for three different models are given in Fig. 12. The minimum and increment values for vorticity

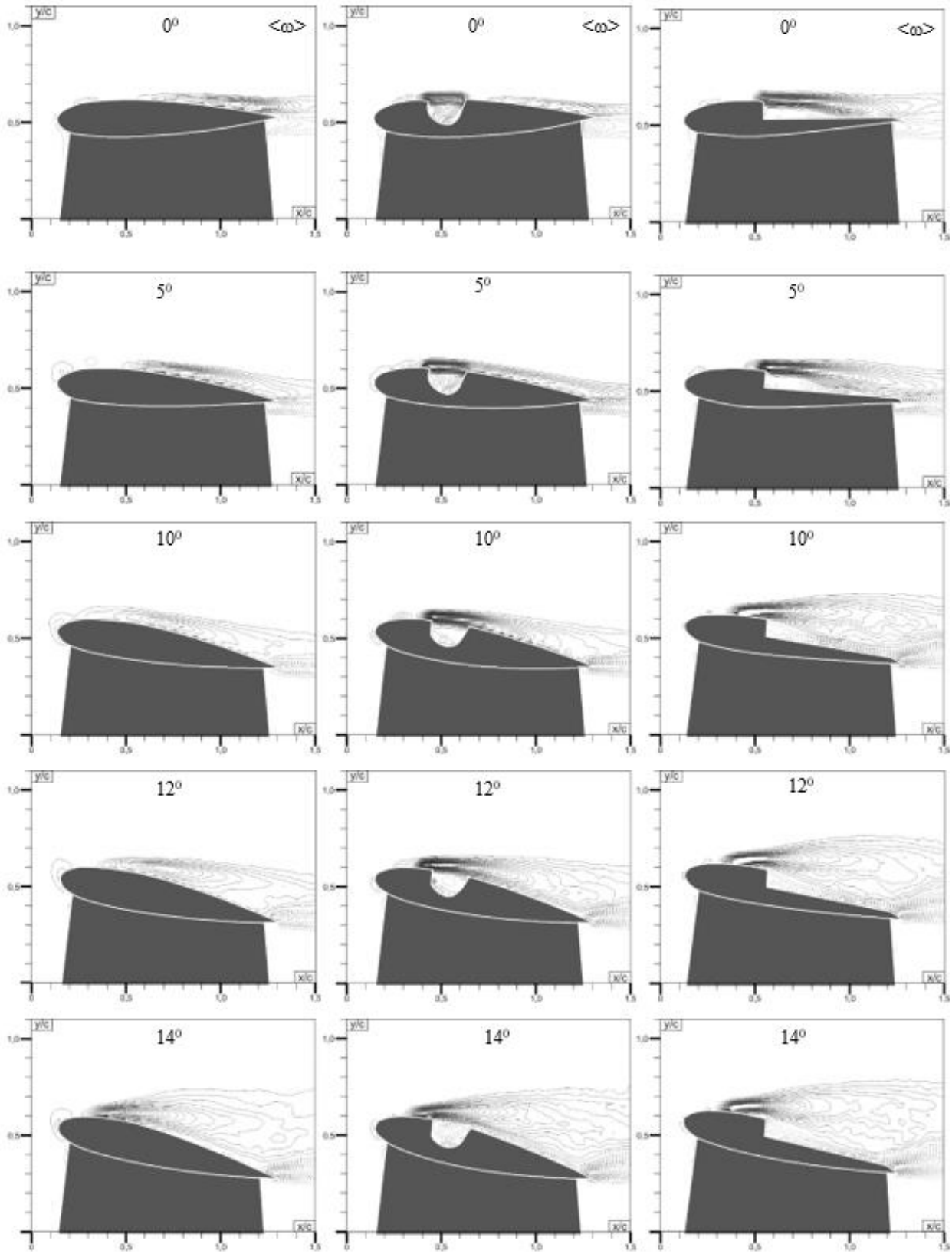

A B C

Fig. 12 Time-averaged vorticities at different angle attack of A) standard model, B) gapped model, C) stepped model

contours <w>, were taken as ±1 and 1, respectively. The flow separation point and the formed vortex shape differ in each model and each angle of attack. In airfoil structures modified according to the standard model, vortex aggregation at small attack angles is seen at the modification points, while this aggregation is transported to the front region of the airfoil as the angle of attack increases. Furthermore, the vortex region is wider in the

stepped model compared to both the gapped and standard models. In addition, the vortex area increases with increasing angle of attack. The largest vortex area is seen at the stepped model with a 14º attack angle, while the smallest is at the standard model with a 0º attack angle.

The pressure contours obtained numerically in different airfoil structures are given in Fig. 13. The static pressure value at the suction part of the section is smaller than the static pressure value at the lower part. Thus, a lifting force occurs due to the resulting pressure difference. The lower the pressure in the suction part and the higher the pressure in the lower part, the higher the lift force occurs. In the visuals given in Fig. 13, the blue regions show the places where the static pressure value is low. It shows the places where the static pressure is higher in the red, yellow, or green regions than in the blue regions. At the front end of the airfoil sections, static pressure is shown in red. At this point, the flow velocity has reached zero and the static pressure has reached its highest value. As the angle of attack increases, the colour of the area at the lower part of the airfoil section changes to yellow colour. These changes are evaluated as the increase in the static pressure value (and therefore increasing the pressure difference and the lifting force). These results are also consistent with the C_D and C_L variation graphs obtained with respect to the angle of attack shown in Fig. 14 and Fig. 15.

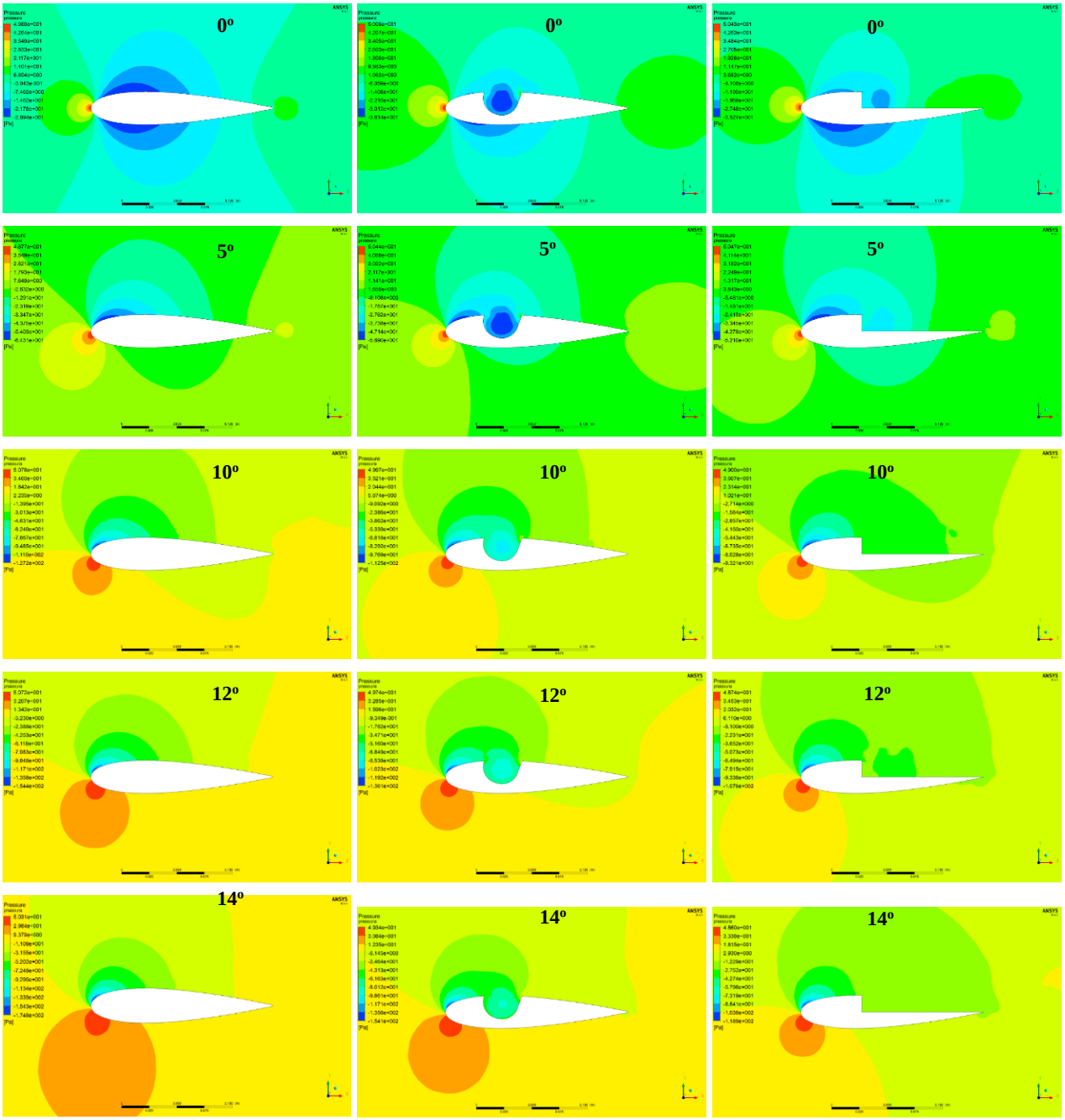

A B C

Fig. 13 Pressure contours at different angle attack of A) standard model, B) gapped model, C) stepped model

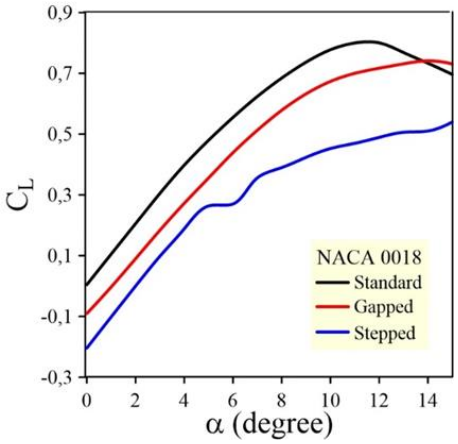

Fig. 14 Change of C_L value versus angle of attack for three airfoils models

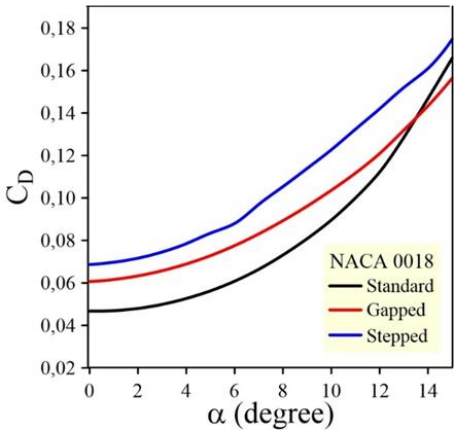

Fig. 15 Change of C_D value versus angle of attack for three airfoils models

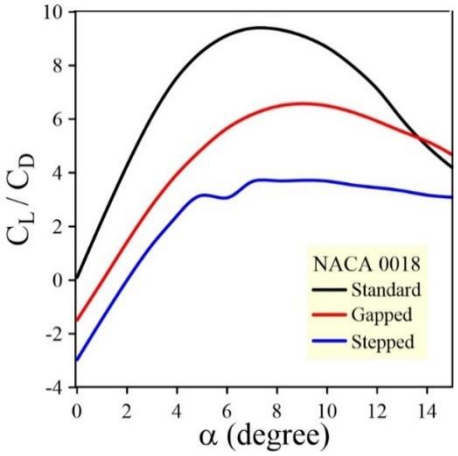

Fig. 16 Change of C_L/C_Dvalues as a function of the attack angle for three airfoils models

One of the most important parameters investigated in airfoil aerodynamic structures is the stall event. The stall causes a decrease in lift coefficient created by an airfoil as the angle of attack increases. The critical angle of attack is in the range of approximately 8-20 degrees, depending on the airfoil geometry, fluid type, and Reynolds numbers. When the stall arises, the airfoil produces less lift and more drag. In C_L – α graphs, the peak points out the angle of the stall. The changes of C_L, C_D and C_L / C_D values obtained by numerical results for Re = $2x10^4$ depending on the angle of attack are presented in Figs 14, 15 and 16, respectively. All C_L and C_D values have been obtained in the range of 0-15 degrees to reveal that values of C_L and C_D strongly depend on the angles of attack. When the pressure contours of the gapped and stepped wing model are examined, it is seen that, unlike the standard wing profile, initially, the pressure on the pressure surface is lower than the suction surface, and an increase in angle of attack reverses this pressure variation. It is clearly seen that for the same angle of attack, the standard model has the highest C_L value while the stepped model has the lowest, as seen in the variation of "C_L - α (angle of attack)" in Figure 14. Furthermore, while the standard model experienced stall after α = 11º of attack angle, the gapped model started to stall after α = 14º. It was observed that C_L curves of all models had the same slope in the range of α = 0º -5º angle of attack range, but the C_L distribution of the stepped model followed a different path in the range of α = 5º -7º and α = 14º -15º attack range.

The change of C_D versus the angle of attack graphs is illustrated in Fig. 15. It is seen that all models behave in the same manner for the small values of the angle of attack. The highest and lowest values are observed for the stepped and standard models. However, the standard model has the lowest values in the range of angle of attack α = 0º -13.5º, while the gapped model has the lowest values in the range of angle of attack of α = 13.5º -15º.

C_L/C_D as a function of the angle of attack graphs is given in Fig. 16. It is clearly seen that the highest values belonging to the standard model take place in the range of angle of attack α = 0º -13.5º, and the lowest values belonging to the stepped model occur for the same range of angles. In the angles of attack range of α = 13.5º -15º, the gapped model has a higher value than the standard model. Maximum C_L/C_D values are observed at α =7º for the standard model, at α =9º for the gapped model, and in the range of α=7º - 9º for the stepped model. In addition, the stepped model shows a slower change after α=5°.

4. CONCLUSION

In this study, experimental and numerical analyses of the standard, gapped, and stepped NACA 0018 airfoil models at different angles of attack were performed. The PIV technique, which is one of the most preferred methods in the literature in recent years, has been used for experimental analysis, and the ANSYS Fluent software, which has been preferred in many studies of CFD analysis for many years, has been used for numerical analysis. Time-average velocity vectors, streamlines, and vorticity contours of the flow fields of the models were obtained from the experiments. At different attack angles, numerical studies provided time-averaged streamlines, pressure contours, and lift, drag and lift/drag ratio values.

While the experimental analyses were made at Re = $2x10^4$ due to physical limitations, numerical

studies were also made in the same range of Re number in order to make comparisons. In order to show the accuracy of the results obtained from the numerical analysis, the C_L values were compared with the work of Gerakopulos et al. (2010). As a result, it has been seen that the numerical results are consistent with the experimental results.

The final conclusions are listed below:

- It was observed that the flow separation according to the streamlines obtained from the experimental results occurred at $\alpha = 12^o$ in the standard model, $\alpha = 10^o$ in the gapped model, and $\alpha = 5^o$ in the stepped model. In the gapped and stepped model, it was observed that in addition to the vorticity concentrations formed on the airfoil, there were also vorticity concentrations in the cavity and the step, and more than one vorticity was formed at some angles of attack. Compared to the other two models, the biggest change depending on the angle of attack is seen in the stepped model. At low angles of attack, it was seen that vorticity contours were concentrated just above the gap and the step in the gapped and stepped models. At high angles of attack, vorticity contours were concentrated at the flow separation point in all models.
- It was seen that flow separation started after the angle of attack of $\alpha = 10^o$ in the standard model. On the other hand, it was observed that the flow separation started after $\alpha = 5^o$ in the gap model and in the stepped model.
- When the time average pressure contours due to the change of angle of attack of all models are examined, it is seen that the maximum pressure difference between the pressure surface and the suction surface of the airfoil profile is the standard, gapped, and then stepped model at all attack angles, respectively.
- Unlike the standard model, it is observed that the pressure on the bottom surface is lower than the top surface at the beginning ($\alpha = 0^o$) and this pressure difference reverses as the angle of attack increases in the gapped and stepped model. This can be clearly seen in the C_L - angle of attack graph for the stepped model. The C_L value is negative in the stepped model up to $\alpha = 2^o$ angle of attack and positive at a higher angle of attack. This situation occurred approximately $\alpha = 1^o$ for the gapped model. While the standard model experienced the stall after the angle of attack α=12°, the stall of the gapped model began after α=14°. It is observed that the C_L value decreases suddenly after α=12° in the standard model, and the values of the other two models are more stable. It was seen that C_L values of all models had the same rate α=0-5° attack angle range, but there is stability in the C_L value of the stepped model in the range α=5°-7°. When the results of C_L versus the angle of attack are examined, it is seen that the standard model has the highest and the stepped model has the lowest values in the same angle of attack. These features allow these models to be used for different purposes.
- The gap and the step opened on the airfoil surface have affected the flow structure. However, this effect is not positive in terms of lift compared to the standard model. It has been observed that the gapped model has a better performance than the stepped model. Up to $\alpha = 10^o$, a slower increase in C_D value was observed for all models, by increasing the attack angle, the drag appeared to increase faster. The C_D value of the standard model has the lowest amount in the range of attack angle α=0- 13.5^o, whereas this value is greater than the amount of the gapped model in the range of attack angle α=13.5-15^o.
- When the C_L / C_D rate corresponding to the angle of attack is examined, it is seen that the highest values belong to the standard model in the range of α =0-13.5^o, and the lowest values belong to the stepped model at all the angles of attack. In the α=13.5-15°, attack angle range, the gapped model has a higher value than the standard model, and this C_L / C_D value of the stepped model shows a slower change after α=5^o.
- It was obtained the highest C_L value is 0.8 at α=12 attack angle in the standard airfoil, the highest C_D value is 0.17 with α=15 attack angle in the stepped airfoil, the highest C_L /C_D value is 9.39 at angles of attack, α=7 degree for the standard airfoil.

ACKNOWLEDGEMENTS

The authors gratefully acknowledge the Mechanical Engineering Department of Cukurova University, Adana, – Turkey, for providing a PIV testing facility for the present work. This study was supported by Cumhuriyet University Scientific Research Projects (CUBAP) with project number M-496.

CONFLICT OF INTEREST

The authors declare that they have no conflict of interest.

AUTHORS CONTRIBUTION

Adnan Öztürk: Supervision, Conceptualization, Methodology, **Mehmet Çoban**: Validation, Formal analysis, Investigation, Writing- Original draft preparation. **Ferhat KOCA**: Validation, Visualization, Investigation, Writing- Reviewing and Editing

REFERENCES

Anzalotta, C., Joshi, K., Fernandez, E., & Bhattacharya, S. (2020). Effect of forcing the tip-gap of a NACA0065 airfoil using plasma actuators: A proof-of-concept study. *Aerospace Science and Technology*, 107, 106268.

https://doi.org/10.1016/j.ast.2020.106268

Belamadi, R., Djemili, A., Ilinca, A., & Mdouki, R. (2016). Aerodynamic performance analysis of slotted airfoils for application to wind turbine blades. *Journal of Wind Engineering and Industrial Aerodynamics*, 151(4), 79-99. https://doi.org/10.1016/j.jweia.2016.01.011

Bhattacharya, S., & Gregory, J. W. (2015). Investigation of the cylinder wake under spanwise periodic forcing with a segmented plasma actuator. *Physics of Fluids*, 27(1), 014102. https://doi.org/10.1063/1.4905536

Choudhry, A., Arjomandi, M., & Kelso, R. (2015). A study of long separation bubble on thick airfoils and its consequent effects. *International Journal of Heat Fluid Flow*, 52(4), 84-96. https://doi.org/10.1016/j.ijheatfluidflow.2014.12.001

Counsil J. N. N. & Boulama, K. G. (2013). Low-reynolds-number aerodynamic performances of the NACA 0012 and selig–donovan 7003 airfoils. *Journal of Aircraft*, 50(1), 204-216. https://doi.org/10.2514/1.C031856

Esfahani, J. A., Barati, E., & Karbasian, H. R. (2015). Fluid structures of flapping airfoil with elliptical motion trajectory. *Computers & Fluids*, 108, 142-155. https://doi.org/10.1016/j.compfluid.2014.12.002

Fouatih, O. M., Medale, M., Imine, O., & Imine, B. (2016). Design optimization of the aerodynamic passive flow control on NACA 4415 airfoil using vortex generators. *European Journal of Mechanics-B/Fluids*, 56, 82-96. https://doi.org/10.1016/j.euromechflu.2015.11.006

Genc, M. S., Özışık, G., & Kahraman, N. (2008). Investigation of aerodynamics performance of NACA0012 aerofoil with plain. *Journal of Thermal Science and Technology*, 28 (1) 1-8. ISSN 1300-3615.

Gerakopulos, R., Boultilier, M., & Yarusevych, S. (2010). *Aerodynamic characterization of a NACA 0018 airfoil at low Reynolds number*. 40th Fluid Dynamics Conference and Exhibit America Institute of Aeronautics and Astronautics. https://doi.org/10.2514/6.2010-4629

Guoqiang, L., Weiguo, Z., Yubiao, J., & Pengyu, Y. (2019). Experimental investigation of dynamic stall flow control for wind turbine airfoils using a plasma actuator. *Energy*, 185, 90-101. https://doi.org/10.1016/j.energy.2019.07.017

Han X. & Krajnović, S. (2015). Very-Large-Eddy simulation based on k-ω model. *AIAA Journal*, 53(4), 1103-1108. https://doi.org/10.2514/1.J053341

He, X., Wang, J., Yang, M., Ma, D., Yan, C., & Liu, P. (2016). Numerical simulation of Gurney flap on SFYT15thick airfoil. *Theoretical and Applied Mechanics Letters*, 6(6), 286-292. https://doi.org/10.1016/j.taml.2016.09.002

Hoogedoorn, E., Jacobs, G. B., & Beyene, A. (2010). Aero-elastic behavior of a flexible blade for wind turbine application: A 2D computational study. *Energy*, 35(2), 778-785. https://doi.org/10.1016/j.energy.2009.08.030

Jawahar, H. K., Ai, Q., & Azarpeyvand, M. (2018). Experimental and numerical investigation of aerodynamic performance for airfoils with morphed trailing edges. *Renewable Energy*, 127, 355-367. https://doi.org/10.1016/j.renene.2018.04.066

Joshi, K., & Bhattacharya, S. (2019). Large-eddy simulation of the effect of distributed plasma forcing on the wake of a circular cylinder. *Computers & Fluids*, 193, 104295. https://doi.org/10.1016/j.compfluid.2019.104295

Koca, F., & Ozturk, A. (2022). Experimental investigation of the effect of a semi-circular spiral protrusion on the turbulent flow past a cylinder. *Fluid Dynamics*, 57, 371–386. https://doi.org/10.1134/S0015462822030089

Lin, J. C. (2002). Review of research on low-profile vortex generators to control boundary-layer separation. *Progress in Aerospace Sciences*, 38 (4-5), 389-420. https://doi.org/10.1016/S0376-0421(02)00010-6

Luo, D., Huang, D., & Sun, X. (2017). Passive flow control of a stalled airfoil using a microcylinder. *Journal of Wind Engineering and Industrial Aerodynamics*, 170, 256-273. https://doi.org/10.1016/j.jweia.2017.08.020

Mertinez-Muriel, C., & Flores, O. (2020). Analysis of vortical gust impact on airfoils at low Reynolds number. *Journal of Fluids and Structures*, 99, 103138-103152. https://doi.org/10.1016/j.jfluidstructs.2020.103138

Orabi, M. Y. A., Elbaz, A. M. R., Mahmoud, N. A. & Hamed, A. M. (2020). Computational modeling of transitional flow over NACA-0018 airfoil at low Reynolds Number. *International Journal of Advance Research, Ideas and Innovations in Technology*, 6(6), 241-265.

Olsman, W. F. J., Willems, J. F. H., Hirschberg, A., Colonius, T., & Trieling, R. R. (2011). Flow around a NACA0018 airfoil with a cavity and its dynamical response to acoustic forcing. *Experiments in Fluids*, 51, 493–509. https://doi.org/10.1007/s00348-011-1065-7

Ozturk, A., & Coban, M. (2014). Experimental investigation of the effect of the vortex trap on an airfoil profile on flow structure, *V. National Aeronautics and Space Conference*, 069, 1-14.

Rubel, R. I., Uddin, K., Islam, Z., & Rokunuzzaman, M.

D. (2017). Numerical and experimental investigation of aerodynamics characteristics of NACA 0015 aerofoil. *International Journal of Engineering Technologies IJET*, 2(4), 132-141. https://doi.org/10.19072/ijet.280499

Sreejith, B. K., & Sathyabhama, A. (2018). Numerical study on effect of boundary layer trips on aerodynamic performance of E216 airfoil. *Engineering Science and Technology, an International Journal*, 21(1), 77-88. https://doi.org/10.1016/j.jestch.2018.02.005

Sun, Z., Mao, Y., & Fan, M. (2021). Performance optimization and investigation of flow phenomena on tidal turbine blade airfoil considering cavitation and roughness. *Applied Ocean Research*, 106, 102463-102479. https://doi.org/10.1016/j.apor.2020.102463

Tanürün, H. E., Ata, İ., Canlı, M. E. & Acır, A. (2020). Numerical and experimental investigation of NACA-0018 wind turbine aerofoil model performance for different aspect ratios. *Journal of Polytechnic*, 23(2), 371-381. https://doi.org/10.2339/politeknik.500043

Wang, J., Zang, C., Wu, Z., Wharton, J., & Luquan, R. (2017). Numerical study on reduction of aerodynamic noise around an airfoil with biomimetic structures. *Journal of Sound and Vibration*, 394, 46-58. https://doi.org/10.1016/j.jsv.2016.11.021

Wilcox, D. C. (1988). Reassessment of the scale-determining equation for advanced turbulence models, *AIAA Journal*, 26(11), 1299-1310. https://doi.org/10.2514/3.10041

Yadav, R., & Bodavula, A. (2021). Numerical investigation of the effect of triangular cavity on the unsteady aerodynamics of NACA 0012 at A low reynolds number. *Proceedings of the Institution of Mechanical Engineers, Part G: Journal of Aerospace Engineering*, 236(6), 1-17. https://doi.org/10.1177/09544100211027042

Yang, Y., Li, C., Zhang, W., Guo, X., & Quanyong, Y. (2017). Investigation on aerodynamics and active flow control of a vertical axis wind turbine with flapped airfoil. *Journal of Mechanical Science and Technology* 31, 1645–1655. https://doi.org/10.1007/s12206-017-0312-0

Yavuz, M. M. (2021). Flow and mechanical characteristics of a modified naca wing geometry. *Çukurova University Journal of the Faculty of Engineering*, 36(3), 815-825. https://doi.org/10.21605/cukurovaumfd.1005807

Zhang, X., Wang, G., Zang, M., Liu, H., & Li, W. (2017). Numerical study of the aerodynamic performance of blunt trailing-edge airfoil considering the sensitive roughness height. *International Journal of Hydrogen Energy*, 42 (29), 18252-18262. https://doi.org/10.1016/j.ijhydene.2017.04.158